

# Density Matrix Renormalization Group in the Heisenberg Picture

Michael J. Hartmann<sup>1,2,3,\*</sup>, Javier Prior<sup>2,3,4</sup>, Stephen R. Clark<sup>4,5</sup>, and Martin B. Plenio<sup>2,3</sup>

<sup>1</sup> *Technische Universität München, Physik Department I, James Franck Str., 85748 Garching, Germany*

<sup>2</sup> *Institute for Mathematical Sciences, Imperial College London, SW7 2PG, United Kingdom*

<sup>3</sup> *QOLS, The Blackett Laboratory, Imperial College London, London SW7 2BW, United Kingdom*

<sup>4</sup> *Clarendon Laboratory, University of Oxford, Parks Road, Oxford OX1 3PU, United Kingdom and*

<sup>5</sup> *Centre for Quantum Technologies, National University of Singapore, 3 Science Drive 2, Singapore 117543, Singapore*

(Dated: November 1, 2018)

In some cases the state of a quantum system with a large number of subsystems can be approximated efficiently by the density matrix renormalization group, which makes use of redundancies in the description of the state. Here we show that the achievable efficiency can be much better when performing density matrix renormalization group calculations in the Heisenberg picture, as only the observable of interest but not the entire state is considered. In some non-trivial cases, this approach can even be exact for finite bond dimensions.

PACS numbers: 03.67.Mn, 02.70.-c, 75.10.Pq

*Introduction* – Quantum many-particle systems give rise to a number of intriguing phenomena such as quantum phase transitions, magnetic frustration, the existence of rare-earth magnetic insulators or high-temperature superconductivity. But as the size of the Hilbert space grows exponentially with the number of subsystems, the numerical simulation of such quantum many-body systems is difficult and often intractable.

In some cases, however, a quantum system does not explore its entire Hilbert space and numerical approaches like the *density-matrix renormalization group* (DMRG) technique [1], become efficient tools. DMRG can be understood as a variation over the set of *matrix product states* (MPS) [2, 3] whose size grows only polynomially with the number of subsystems. Its success is linked to the existence of an upper bound for the entanglement of contiguous sub-blocks of the system under study [4, 5, 6]. This approach is therefore expected to work particularly well for the ground state of one-dimensional gapped systems, in which correlation functions decay exponentially and the entanglement entropy saturates, satisfying an “area law” [6, 7]. There are of course situations in which no upper bound to the entanglement in the system exists or where it grows in time. In such cases the performance of DMRG deteriorates. This is typically the case for the dynamics of non-equilibrium states, as exemplified in recent studies of sudden quenches to Bose-Hubbard Hamiltonians [8]. Due to its dynamical production, the entanglement per unit area may grow linearly in time in those scenarios [9, 10]. To achieve a fixed precision DMRG algorithms hence need to use matrix dimensions that grow exponentially in time rendering them inefficient [10].

An increasing number of experimental settings, including arrays of Josephson junctions [11], ultra cold atoms in optical lattices [12], ion traps [13] and arrays of coupled micro-cavities [14], offer the possibility to generate effective many-particle systems. Hence, dynamical studies of quantum many-particle systems are expected to receive increasing attention in the future. Moreover in real ex-

perimental situations, such systems will typically suffer from decoherence and dissipation and hence evolve into mixed states whose numerical description is even more demanding. It is therefore desirable to develop new more efficient methods for such problems or alternatively to improve existing DMRG methods further.

In this letter we describe an approach to enhance the performance of DMRG in time-dependent settings by computing directly the observable of interest and propagating its evolution in the Heisenberg picture. Our approach avoids calculating components of the quantum states that are irrelevant to the observable of interest and hence contrasts the standard DMRG approach, which generates a quantum state for the entire quantum system in the Schrödinger picture. DMRG performed in the Heisenberg and Schrödinger picture are thus complementary. Whereas Schrödinger picture simulations calculate the entire state and subsequently allow to compute any observable of interest, Heisenberg picture calculations only consider one operator whose expectation value can in turn be computed for any initial state.

In the sequel, we demonstrate that DMRG performed in the Heisenberg picture (H-DMRG) can have significant advantages for numerical simulations of quantum many-particle dynamics. These advantages become most significant in open system dynamics described by mixed states but can also be demonstrated rigorously for certain exactly solvable systems. We find numerical indications for a saturation of the block entanglement in the Heisenberg picture for increasing system size which suggest that H-DMRG has superior efficiency in many cases.

*Main part* – For linear chains of interacting subsystems, we consider the evolution of operators such as  $\mathcal{X}_m(t) = U(t) (\mathbb{1}^{\otimes m-1} \otimes \mathcal{X} \otimes \mathbb{1}^{\otimes N-m}) U(t)^\dagger$ , where  $\mathcal{X}$  is a Hermitian operator acting on site  $m$ , and use a matrix-product representation

$$\mathcal{X}_m = \sum_{i_1, \dots, i_N=0}^3 \text{tr} [A_{i_1}^{(1)} \dots A_{i_N}^{(N)}] P_{i_1} \otimes \dots \otimes P_{i_N} \quad (1)$$

with suitable  $d \times d$ -dimensional matrices  $A_i^{(l)}$  and the canonical operator basis  $\{P_0, P_1, P_2, P_3\}$  with  $(P_m)_{i,j} = \delta_{m,2i+j}$  for  $i, j \in \{0, 1\}$ . We focus our study on dynamics of the anisotropic Heisenberg Hamiltonian for a chain of  $N$  spins,

$$H = \sum_{j=1}^N B_z \sigma_j^z + \sum_{j=1}^{N-1} \sum_{\alpha=x,y,z} J_\alpha \sigma_j^\alpha \sigma_{j+1}^\alpha, \quad (2)$$

as this model is known to exhibit dynamics that is numerically hard to simulate. In eq. (2),  $B_z$  is an applied magnetic field,  $J_x, J_y$  and  $J_z$  are spin-spin couplings and  $\sigma_j^x, \sigma_j^y$  and  $\sigma_j^z$  the Pauli operators at site  $j$ .

*Exact results* – It is noteworthy that the time evolution of certain operators can actually be represented *exactly* by a matrix product operator with fixed finite bond dimension. For Hamiltonians of the form of eq. (2) with  $J_z = 0$ , all local operators that transform under the Jordan-Wigner transformation [15] into local fermionic operators remain exact matrix product operators with fixed finite dimension for all times. Examples of such operators are  $\sigma_m^z$  whose time evolution is an exact matrix product operator for matrix dimension  $d = 4$  and generally any product of Pauli-operators with an even number of  $\sigma^x$  or  $\sigma^y$  operators and any number of  $\sigma^z$  operators.

To see this, let us first define the fermionic annihilation and creation operators [15],  $c_m = \prod_{j=1}^{m-1} \sigma_j^z (\sigma_m^x + i\sigma_m^y)/2$ . In terms of  $c_m$  and  $c_m^\dagger$ , the Hamiltonian (2) with  $J_z = 0$  reads  $H = -B \sum_{j=1}^N (2c_j^\dagger c_j - 1) + J_x \sum_{j=1}^{N-1} (c_j^\dagger - c_j)(c_{j+1}^\dagger + c_{j+1}) - J_y \sum_{j=1}^{N-1} (c_j^\dagger + c_j)(c_{j+1}^\dagger - c_{j+1})$ . Given that the Hamiltonian is quadratic in  $c_m$  and  $c_m^\dagger$ , the Heisenberg time evolution of an individual Heisenberg operator such as  $c_m(t)$  is found to be  $c_m(t) = \sum_{j=1}^N (\alpha_j(t)c_j + \beta_j(t)c_j^\dagger)$ . In the fermionic picture this may be written as matrix product operator with matrices of dimension 2 as it is essentially the same as a W-state. Rewriting the rhs in terms of Pauli operators we find  $c_m(t) = \sum_{j=1}^N (\alpha_j(t) \prod_{l=1}^{j-1} \sigma_l^z \sigma_j^+ + \beta_j(t) \prod_{l=1}^{j-1} \sigma_l^z \sigma_j^-)$ , where  $\sigma^\pm = \frac{1}{2}(\sigma^x \pm i\sigma^y)$ . This in turn may be written as a matrix product operator of the form eq. (1) whose matrices have the structure  $A_0^{(1)} = P_1, A_0^{(m)} = P_0 + P_3, A_0^{(N)} = P_0, A_1^{(1)} = \alpha_1(t)P_0, A_1^{(m)} = \alpha_m(t)P_2, A_1^{(N)} = \alpha_N(t)P_2, A_2^{(1)} = \beta_1(t)P_0, A_2^{(m)} = \beta_m(t)P_2, A_2^{(N)} = \beta_N(t)P_2, A_3^{(1)} = -P_1, A_3^{(m)} = P_0 - P_3, A_3^{(N)} = P_0$ .

As every spin operator may be expressed as a sum of products of fermionic operators we can now understand the above observations. For example, because  $\sigma_m^z = 2c_m^\dagger c_m - 1$  we can write it as a product of two matrix product operators each with dimension 2, so that  $\sigma_k^z$  is a matrix product operator with dimension at most 4. This reasoning also holds for models with disorder, i.e. where the magnetic field or the couplings depend on the lattice site ( $B_z(j), J_x(j)$  and  $J_y(j)$ ), which can not be diagonalized via Fourier and Bogolubov transformations

[15]. Analogous conclusions hold for quasi-free bosonic systems.

This observation demonstrates that a DMRG simulation in the Heisenberg picture may be considerably more efficient, even exact, in cases where the same approach in the Schrödinger picture is provably inefficient [10]. In contrast to the Schrödinger picture, the block entanglement in the Heisenberg picture (considering the four operators  $P_0, P_1, P_2, P_3$  as basis-vectors of a 4-dim Hilbert space for each site) is bounded for all times. This difference in entanglement scaling in the two pictures obviously can not hold for all settings [18]. Nonetheless we find indications for a saturation in the scaling of block entanglement in numerical simulations for more general models.

*Numerical results* – We now turn to compare the numerical efficiency of H-DMRG with that of DMRG in the Schrödinger picture [1, 2, 3, 4]. For the dynamics of pure states, we have seen that there are examples where DMRG becomes exact thanks to a very favorable behavior of entanglement. In general one expects the use of H-DMRG to be advantageous only where the entanglement scaling for the state is drastically worse than for the operator to be evolved. This is due to the following reason: If a quantum state has the matrix product representation  $|\Psi\rangle = \sum_{i_1 \dots i_N} \text{tr}[A_{i_1}^{(1)} \dots A_{i_N}^{(N)}] |i_1\rangle \otimes \dots \otimes |i_N\rangle$  with matrix dimension  $d$ , then the operator  $|\Psi\rangle\langle\Psi|$  has the matrix product representation

$$|\Psi\rangle\langle\Psi| = \sum_{i_1, \dots, i_N=0}^3 \text{tr}[B_{i_1}^{(1)} \dots B_{i_N}^{(N)}] |i_1\rangle\langle i_1| \otimes \dots \otimes |i_N\rangle\langle i_N|, \quad (3)$$

where  $B_i^{(l)} = A_{i_l}^{(l)} \otimes (A_{i_l}^{(l)})^\dagger$  and hence the  $B$  matrices have dimension  $d^2$ . The matrix product representation of an operator is thus expected to require matrix dimension  $d^2$  in situations, where the representation of a state only requires  $d$  and is therefore much more efficient.

The situation is different if decoherence and dissipation is present as then the evolution of an operator must be considered in both, Heisenberg and Schrödinger picture. Dissipation may be described by local Lindblad terms leading to a master equation for the dynamics of the density matrix  $\rho$  of the form [17],

$$\begin{aligned} \dot{\rho} = & -i[H, \rho] + \sum_{j=1}^N \frac{\Gamma_d}{2} (2\sigma_j^- \rho \sigma_j^+ - \sigma_j^+ \sigma_j^- \rho - \rho \sigma_j^+ \sigma_j^-) \\ & + \sum_{j=1}^N \frac{\Gamma_u}{2} (2\sigma_j^+ \rho \sigma_j^- - \sigma_j^- \sigma_j^+ \rho - \rho \sigma_j^- \sigma_j^+), \end{aligned} \quad (4)$$

where  $\Gamma_d$  and  $\Gamma_u$  are the respective damping rates. When the description is transferred into the Heisenberg picture,

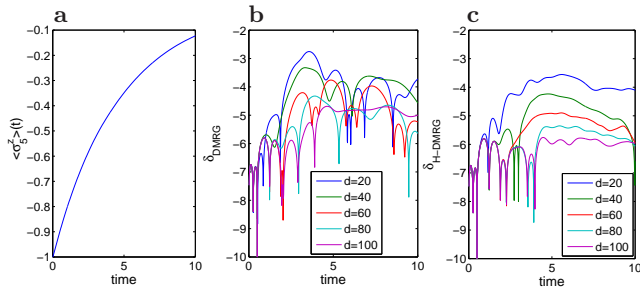


FIG. 1: The time evolution,  $\langle \sigma_5^z \rangle(t)$  for a model described by eqs. (4) respectively (5) with parameters  $N = 10$ ,  $B_z = 0.8$ ,  $J_x = 0.5$ ,  $J_y = 0.4$ ,  $J_z = 0.01$ ,  $\Gamma_u = 0.1$  and  $\Gamma_d = 0.1$ . **a**: The exact solution, **b**:  $\delta_{\text{DMRG}}$  for DMRG-simulations in the Schrödinger picture for  $d = 20$  (blue),  $d = 40$  (green),  $d = 60$  (red),  $d = 80$  (cyan) and  $d = 100$  (magenta), **c**:  $\delta_{\text{H-DMRG}}$  for DMRG-simulations in the Heisenberg picture.

the same dynamics is described by the equation,

$$\dot{\mathcal{X}} = i[H, \mathcal{X}] + \sum_{j=1}^N \frac{\Gamma_d}{2} (2\sigma_j^+ \mathcal{X} \sigma_j^- - \sigma_j^+ \sigma_j^- \mathcal{X} - \mathcal{X} \sigma_j^+ \sigma_j^-) + \sum_{j=1}^N \frac{\Gamma_u}{2} (2\sigma_j^- \mathcal{X} \sigma_j^+ - \sigma_j^- \sigma_j^+ \mathcal{X} - \mathcal{X} \sigma_j^- \sigma_j^+), \quad (5)$$

for a Heisenberg picture operator  $\mathcal{X}(t)$ . In the following we compare the results of numerical simulations in the Schrödinger (eq. 4) [16] and Heisenberg picture (eq. 5).

In our first example we choose the parameters of the model to be,  $N = 10$ ,  $B_z = 0.8$ ,  $J_x = 0.5$ ,  $J_y = 0.4$ ,  $J_z = 0.01$ ,  $\Gamma_u = 0.1$  and  $\Gamma_d = 0.1$  to allow for comparison with exact results. We simulate the time evolution of the operator  $\sigma_5^z(t)$ , where the initial state is all spins pointing down in  $z$ -direction,  $|\phi_0\rangle = |\downarrow, \dots, \downarrow\rangle$  ( $\sigma^z |\downarrow\rangle = -|\downarrow\rangle$ ). Figure 1a shows the exact solution, that is a 2nd order Runge-Kutta integration with time steps  $dt = 0.01$  of eq. (4). All our DMRG simulations also use 2nd order integrations with  $dt = 0.01$ . The errors of DMRG-simulations in the Schrödinger picture,  $\delta_{\text{DMRG}} = \log_{10}(|\langle \sigma_5^z \rangle_{\text{exact}}(t) - \langle \sigma_5^z \rangle_{\text{DMRG}}(t)|)$ , and the Heisenberg picture,  $\delta_{\text{H-DMRG}} = \log_{10}(|\langle \sigma_5^z \rangle_{\text{exact}}(t) - \langle \sigma_5^z \rangle_{\text{H-DMRG}}(t)|)$ , are shown in figures 1b and c respectively (Calculations with time steps  $dt = 0.001$  produced indistinguishable results). The Heisenberg picture simulations show a significantly higher accuracy than the Schrödinger picture results. Moreover the accuracy improvement with increasing matrix dimension  $d$  is more pronounced in the Heisenberg picture, suggesting an unfavorable scaling of entanglement in the Schrödinger picture.

In a second example we consider a chain of  $N = 100$  spins, with slightly different parameters to show the generality of our findings, and compare DMRG results in the Schrödinger and Heisenberg picture. Here,  $B_z = 0.8$ ,  $J_x = 0.5$ ,  $J_y = 0.4$ ,  $J_z = 0.01$ ,  $\Gamma_u = 0.01$  and  $\Gamma_d = 0.1$ .

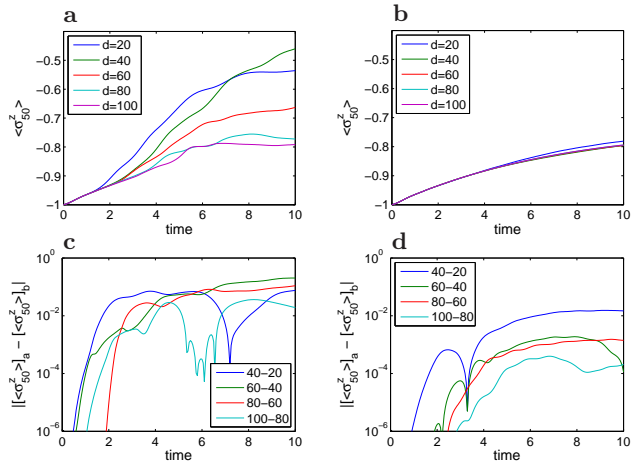


FIG. 2: Dynamics of a chain with  $N = 100$  spins and  $B_z = 0.8$ ,  $J_x = 0.5$ ,  $J_y = 0.4$ ,  $J_z = 0.01$ ,  $\Gamma_u = 0.01$  and  $\Gamma_d = 0.1$ . **a**:  $\langle \sigma_{50}^z \rangle(t)$  as given by eq. (4) (DMRG) for  $d = 20$  (blue),  $d = 40$  (green),  $d = 60$  (red),  $d = 80$  (cyan) and  $d = 100$  (magenta). **b**:  $\langle \sigma_{50}^z \rangle(t)$  as given by eq. (5) (H-DMRG) for  $d = 20, 40, 60, 80$  and  $100$ . **c**:  $|\langle \sigma_{50}^z \rangle(t)_{d1} - \langle \sigma_{50}^z \rangle(t)_{d2}|$  as given by eq. (4) (DMRG) for  $(d1, d2) = (40, 20)$  (blue),  $(d1, d2) = (60, 40)$  (green),  $(d1, d2) = (80, 60)$  (red) and  $(d1, d2) = (100, 80)$  (cyan). **d**:  $|\langle \sigma_{50}^z \rangle(t)_{d1} - \langle \sigma_{50}^z \rangle(t)_{d2}|$  as given by eq. (5) (H-DMRG) for  $(d1, d2) = (40, 20), (60, 40), (80, 60)$  and  $(100, 80)$ . With increasing bond dimension, results converge much faster in the Heisenberg than in the Schrödinger picture.

Figures 2a and 2b show  $\langle \sigma_{50}^z \rangle(t)$  as calculated in the Schrödinger (2a) and Heisenberg picture (2b). Since it is not possible to compare these values to exact results for  $N = 100$ , we test the convergence of the obtained results with increasing matrix dimension,  $d$ . This convergence is shown in figure 2c for the Schrödinger and in figure 2d for the Heisenberg picture, where we plotted the differences between results that were obtained with different matrix dimensions  $d1$  and  $d2$ ,  $|\langle \sigma_{50}^z \rangle(t)_{d1} - \langle \sigma_{50}^z \rangle(t)_{d2}|$ . The convergence is found to be much faster in the Heisenberg than in the Schrödinger picture. We found the advantage of the Heisenberg picture to be of a comparable significance as in figure 2 already for a chain with the same parameters but  $N = 40$  spins.

In our simulations we use the *time evolved block decimation* (TEBD) algorithm introduced in [4]. This algorithm, at each step, truncates the reduced density matrices of all considered bipartitions by only keeping the states corresponding to their  $d$  largest eigenvalues (Here  $d$  is the dimension of the employed matrices.). We compute the truncation error by summing up all truncated eigenvalues of the reduced density matrices [4] at each time step. The truncation errors at each time step,  $\epsilon_t$ , are then cumulatively summed up. The resulting quantity,  $\epsilon = \sum_t \epsilon_t$ , is thus an upper bound to approximation errors due to matrix truncation.

To enable a comparison of the accuracies of the matrix

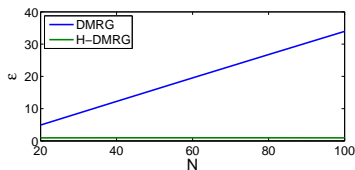


FIG. 3: Truncation errors  $\epsilon$  at  $t = 10$  for Schrödinger picture DMRG (blue) and H-DMRG (green) for  $N = 20, 40, 60$  and  $80$  and fixed bond dimension  $d = 60$ .  $B_z = 0.8$ ,  $J_x = -0.5$ ,  $J_y = 0.4$ ,  $J_z = 0.1$ ,  $\Gamma_u = 0.1$  and  $\Gamma_d = 0.2$ . H-DMRG truncations saturate at  $\epsilon \leq 0.96$ .

truncations, we set Heisenberg and Schrödinger representations on the same footing by normalizing the representations of eqs. (3) and (1) in the Frobenius norm, i.e. for a  $m \times m$  matrix  $X$  we set  $\sum_{i,j=1}^m |X_{i,j}|^2 = 1$ . With this normalization, the matrix representations of  $\varrho$  and  $\mathcal{X}$  both have the structure of Matrix Product States where the eigenvalues of reduced matrices sum up to unity and can be interpreted as Schmidt coefficients[19].

Since we compare truncation errors in two different representations it is not obvious that lower truncation errors in one representation imply a better approximation for the expectation value of an observable or vice versa. Indeed, for the short chains used in the example in figure 1 we found comparable truncation errors in both approaches even though the error in the relevant observable is much smaller when using H-DMRG[20].

On the other hand, the truncation errors appear to be significantly lower in H-DMRG for longer chains. We have therefore investigated the scaling of the truncation error with the system size for fixed bond dimension  $d$ . Importantly, we observe that in contrast to Schrödinger picture DMRG, the truncation errors  $\epsilon$  are found to saturate in H-DMRG for fixed bond dimension if the system size is increased. Figure 3 shows the truncation errors  $\epsilon$  at  $t = 10$  for Schrödinger picture DMRG (blue) and H-DMRG (green) for  $d = 60$  and chain length  $N = 20, 40, 60, 80$  and  $100$ . For the remaining parameters we chose a set, that is again different from those in figures 1 and 2 with  $B_z = 0.8$ ,  $J_x = -0.5$ ,  $J_y = 0.4$ ,  $J_z = 0.1$ ,  $\Gamma_u = 0.1$  and  $\Gamma_d = 0.2$ .

This clear difference in the scaling further corroborates the idea that the Heisenberg and Schrödinger picture are qualitatively different in regards to their entanglement scaling even beyond the exactly solvable models discussed earlier. In fact, this feature hints at a saturation of the entanglement of bipartitions in the Heisenberg picture. It will be an interesting challenge for future work to provide analytical arguments to support the numerical findings presented here and to demonstrate more rigorously the superior efficiency of H-DMRG when applied to mixed state evolutions beyond the numerical findings here.

*Acknowledgements* – This work is part of EU Integrated Project QAP (contract 015848), the EPSRC

QIP-IRC (GR/S82176/0) and the DFG Emmy Noether project HA 5593/1-1. It was supported by EPSRC grant EP/E058256, the Fundación Séneca grant 05570/PD/07 and the Royal Society.

\* Electronic address: michael.hartmann@ph.tum.de

- [1] S.R. White, Phys. Rev. Lett. **69**, 2863 (1992); Phys. Rev. B **48**, 10345 (1993); U. Schollwöck, Rev. Mod. Phys. **77**, 259 (2005).
- [2] M. Fannes, D. Nachtergaele, and R.F. Werner, Commun. Math. Phys. **144**, 443 (1992).
- [3] S. Rommer and S. Ostlund, Phys. Rev. B **55**, 2164 (1997); Phys. Rev. Lett. **75**, 3537 (1995); J. Dukelsky et al., Europhys. Lett. **43**, 457 (1998).
- [4] G. Vidal, Phys. Rev. Lett. **91**, 147902 (2003); G. Vidal, Phys. Rev. Lett. **93**, 040502 (2004).
- [5] T. Prosen and M. Žnidarič, Phys. Rev. E **75**, 015202R (2007); T. Prosen and I. Pižorn, Phys. Rev. E **76**, 032316 (2007).
- [6] J. Eisert, M. Cramer and M.B. Plenio, arXiv:0808.3773, submitted to Rev. Mod. Phys. 2008.
- [7] K. Audenaert et al., Phys. Rev. A **66**, 042327 (2002); I. Peschel, J. Stat. Mech.: Th. Exp. P12005 (2004); B.-Q. Jin and V. E. Korepin, J. Stat. Phys. **116**, 79 (2004); M.B. Plenio et al., Phys. Rev. Lett. **94**, 060503 (2005); M. Cramer et al., Phys. Rev. A **73**, 012309 (2006); M.B. Hastings, J. Stat. Mech.: Th. Exp. P08024 (2007).
- [8] C. Kollath, A. M. Läuchli and E. Altman, Phys. Rev. Lett. **98**, 180601 (2007); M. Rigol et al, Phys. Rev. Lett. **98**, 050405 (2007); M. Cramer et al., Phys. Rev. Lett. **100**, 030602 (2008).
- [9] P. Calabrese and J. Cardy, J. Stat. Mech. 0504, P04010 (2005).
- [10] N. Schuch et al., New J. Phys. **10**, 033032 (2008).
- [11] R. Fazio and H.S.J. van der Zant, Phys. Rep. **355**, 235 (2001).
- [12] I. Bloch, J. Dalibard and W. Zwerger, Rev. Mod. Phys. **80**, 885 (2008); M. Lewenstein et al., Adv. Phys. **56**, 243 (2007).
- [13] D. Porras and J.I. Cirac, Phys. Rev. Lett. **92**, 207901 (2004); A. Retzker et al., arXiv:0801.0623; A. Friede-nauer et al., Nature Phys. **4**, 757 (2008)
- [14] M.J. Hartmann, F.G.S.L. Brandão and M.B. Plenio, Nature Phys. **2**, 849 (2006); D.G. Angelakis, M.F. Santos and S. Bose, Phys. Rev. A **76**, 031805(R) (2007); A.D. Greentree et al., Nature Phys. **2**, 856 (2006).
- [15] E.H. Lieb, T.D. Schultz and D.C. Mattis, Ann. Phys. **16**, 407 (1961).
- [16] M. Zwolak and G. Vidal, Phys. Rev. Lett. **93**, 207205 (2004).
- [17] C. Gardiner and P. Zoller, *Quantum Noise*, Springer (2004).
- [18] It is clear that there must be situations in which also the simulation in the Heisenberg picture must fail. If this was not the case, it would be possible to simulate efficiently quantum algorithms as their final readout consists of single spin measurements only.
- [19] Since this normalization is not preserved by eqs. (4) and (5), the representations need to be renormalized after each time step.

[20] Obviously, the calculated expectation values need to be multiplied by the inverse norms to obtain the physically relevant results.